Twofold Symmetry of Human Fibrinogen Proved at the β Chain Distal Domains by Monoclonal−Immunoelectron Microscopy and Image Analysis†

J. A. Méndez,‡ M. V. Alvarez,§ J. A. Aznárez,‡ and J. González-Rodríguez*,§

Unidad de Biofísica, Instituto de Química Física, CSIC, Serrano 119, E-28006 Madrid, Spain, and Laboratorio de Microscopía Electrónica, Centro de Física, CSIC, Serrano 121, E-28006 Madrid, Spain

Received April 17, 1995; Revised Manuscript Received July 11, 1995⊗

ABSTRACT: Using a murine antibody (F7) specific for the C-terminal domain of the β chain of human fibrinogen combined with electron microscopy and image analysis, we show unequivocally that the epitopes for F7 are at the distal nodules of fibrinogen, equidistant from the center of the molecule and arranged not colinearly with the long axis of the molecule but at opposite sides of it, i.e., following twofold symmetry. Thus, given the monoclonality of the immunochemical probe used and the dimeric nature of the fibrinogen molecule, we can conclude that the distal domains of the two β chains are arranged in the same manner as these epitopes and, therefore, that the fibrinogen molecule has twofold symmetry. This symmetry pattern found here for F7 is the same as that found recently for the platelet fibrinogen receptor binding sites [Weisel, J. W., Nagaswami, C., Vilaire, G., & Bennett, J. S. (1992) *J. Biol. Chem. 23*, 16637-16643], located almost certainly at the C-terminal end of the γ chains, and gives further support to the most accurate model of fibrinogen available so far. We discuss the consequences of this symmetry pattern and of the molecular rigidity of fibrinogen in the actual models of fibrin polymerization and platelet aggregation and adhesion.

Since the early trinodular Hall and Slayter model for fibrinogen was proposed (Halls & Slayter, 1959), based on electron microscopy images of metallically shadowed molecules, the three-dimensional structure of fibrinogen has been controversial and will continue to be so, given the difficulties so far in crystallizing native fibrinogen and in obtaining suitable isomorphous derivative crystals (Rao et al., 1991). The fibrinogen model had always been drawn with a bend (Doolittle, 1984) until Hoeprich and Doolittle (1983) found that the two γ chains[1] and, therefore, the dimeric halves of human fibrinogen are joined through their N-terminal disulfide bonds in an antiparallel orientation, contrary to what had been presumed. Since then, bent and linear models have been used in the literature. Image processing of electron micrographs of native fibrinogen and analysis of crystalline arrays of proteolytically modified fibrinogen by coordinated electron microscopy and X-ray crystallography have led to the development of the most accurate model of fibrinogen so far (Wiesel et al., 1985; Rao et al., 1991). In this model, as before, the central nodule is associated with the N-terminal knot, the two rod-like regions joining the central nodule to the two distal nodules are associated with the α-helical coiled coils, and the distal nodules are associated with the C-terminal domains of the β and γ chains, which in this model are recognized individually as two distal domains. Immunoelectron microscopy has led to the location of the C-terminal domain of the α chains, not normally visible, near the N-terminal disulfide knot (Veklich et al., 1993). Another feature of the model is the arrangement of the C-terminal β and γ domains following a twofold symmetry axis through the center and perpendicular to the long axis of the molecule. This particular feature, which has not been unequivocally proved for fibrinogen in solution, together with the degree of flexibility of the whole molecule (Montego et al., 1992) and of each domain, are bare essentials to understand the molecular mechanism of the hemostatic role of fibrinogen: in blood coagulation (Hunziker et al., 1990; Rao et al., 1991) through the fibrin netwok formation, and in platelet adhesion to subendothelium and platelet−platelet aggregation (Hawiger et al., 1989; Weisel et al., 1992) through the interaction with its receptor (the glycoprotein IIb/IIIa or integrin α_{IIb}/β_3) at the surface of blood platelets.

In the present work, we use monoclonal antibodies specific for the two distal nodules of fibrinogen combined with electron microscopy and image analysis to prove unequivocally that the distal domains in fibrinogen are arranged following a twofold symmetry axis going through the center and perpendicular to the long axis of the molecule. We discuss the consequences of this feature in the actual models of fibrin polymerization and platelet aggregation and adhesion.

MATERIALS AND METHODS

Materials

(A) Human fibrinogen (Kabi, Stockholm) was fractionated in a Sephacryl S-400 HR column (2.6 × 90 cm) equilibrated in 20 mM sodium phosphate, 130 mM sodium chloride, and 0.025% sodium azide, pH 7.4. The fractions of the main band were analyzed by SDS−PAGE under reduced and nonreduced conditions and subjected to thrombin coagula-

† Supported by the DGICYT (Grants PM 90-145 and PM 92-04) and FIS (95/1806).

* To whom correspondence should be addressed. E-mail ROCJGR@ROCA.CSIC.ES; Fax 34.1.564 2431.

‡ Centro de Física.

§ Instituto de Química Física.

⊗ Abstract published in *Advance ACS Abstracts,* December 1, 1995.

[1] Abbreviations: α, β, and γ chains, the three constituent chains making the hemimolecule of fibrinogen; GPIIb/IIIa or integrin $\alpha_{IIb}\beta_3$, heterodimer of glycoproteins IIb (α_{IIb}) and IIIa (β_3); IgG, immunoglobulin G.

0006-2960/96/0435-634$12.00/0

tion, to assess the degree of purity, the integrity of its constituent chains, and clottability (>94%), before storage at −120 °C. The fibrinogen concentration was measured spectrophotometrically using extinction coefficient $E_{280}^{0.1\%} = 1.51$.

(B) Individual Fibrinogen Chains. Purified human fibrinogen in 0.1 M Tris-HCl and 0.1% SDS, pH 8.5 buffer was reduced for 2 h with a 100-fold molar excess of dithioerythritol over the theoretical content of cysteine in fibrinogen, followed by alkylation for 2 h in the dark with a 1.5-fold molar excess of 4-vinylpyridine with respect to the dithioerythritol added. The sample was extensively dialyzed against 50 mM Tris-HCl, 0.1% SDS, and 0.025% sodium azide, pH 7.4 buffer and finally subjected to reverse phase chromatography either on a Vydac C_4 protein/peptide RP column (5 μm, 250 × 4.6 mm) or on a column (100 × 5 mm) of modified polystyrene−divinylbenzene packing POROS 20, to isolate the reduced and alkylated α, β, and γ chains of fibrinogen.

(C) Monoclonal Antibodies. Murine monoclonal antibodies anti-human fibrinogen (F2, F5, F6, F7, F8, F9, and F12), all of the IgG class, were prepared according to immunization and fusion protocols and screening assays described previously (Melero & Gonzalez-Rodriguez, 1984). Antibodies were purified from ascitic fluids after sequential 25% and 50% saturated $(NH_4)_2SO_4$ precipitation. The 50% saturated $(NH_4)_2SO_4$ precipitates were subjected to affinity chromatography on protein A−Sepharose (Pharmacia, Sweden) according to the manufacturer's instructions. The purification process was monitored by SDS−PAGE and enzyme immunoassay, using fibrinogen adsorbed at the bottom of the wells and as second antibody a goat anti-(mouse IgG) IgG. The antibody concentration was measured spectrophotometrically using extinction coefficient $E_{280}^{0.1\%} = 1.36$.

Methods

(A) Preparation and Fractionation of the Fibrinogen−Monoclonal Antibody Complexes. Purified human fibrinogen (6 μM) was mixed with a 2- to 4-fold molar excess of monoclonal antibody in a final volume of 50 μL, and the mixture was incubated at 4 °C overnight. Then the supernatant after centrifugation at 13 000 rpm for 10 min was loaded into a Sephacryl S-400 HR column (1 × 50 cm) equilibrated in 100 mM Tris-HCl and 0.025% sodium azide, pH 7.4. The fractions along the elution profile were analyzed by SDS−PAGE (Laemmli, 1970), and their protein concentration was determined by the method of Markwell et al. (1978). The identified fractions of the fibrinogen−monoclonal antibody complexes were used for electron microscopy.

(B) Characterization of the Monoclonal Antibodies. The affinity of the antibodies for fibrinogen was measured by enzyme immunoassay following the method of Friguet et al. (1985). The identification of the reduced and the reduced and alkylated fibrinogen chain recognized by each antibody was done by immunoelectroblotting (Towbin et al., 1979).

The inhibition of fibrin formation was assessed by measuring the fibrinogen clottability by thrombin at a fibrinogen/monoclonal antibody ratio of 1.

(C) Electron Microscopy of Metal Rotary Shadowed Samples. Protein samples (5−20 μg/mL) in a 2/1 buffer/glycerol mixture were prepared for electron microscopy observation by rotary shadowing at very low angle as described before (Rivas et al., 1991). About 50 μL of the protein was sprayed at a 50 cm distance onto a 1 cm^2 piece of freshly cleaved mica, which was immediately transferred into a BAE 300 Balzers unit and dried for 60 min at 10^{-6} Torr. The dehydrated samples were further shadowed with a 0.5−0.6 nm thick platinum/carbon film at a 5° angle and backed with a 15 nm thick carbon layer. Replicas were floated on water and mounted on grids. Observation was carried out in a Siemens Elmiskop 1A at 80 kV, and micrographs were taken at 40000× magnification.

(D) Analysis of the Electron Micrographs. Individual objects in photographic film were subjected to scanning optical densitometry at 5 μm resolution for IgG and at 10 μm resolution for fibrinogen and the fibrinogen−antibody complexes, using a Perkin Elmer microdensitometer model PDS and generating data matrices of 240 × 240 and 400 × 400, respectively. The digitized data corresponding to several hundred individual objects of each class were transferred to a DECpc αXP 150 work station and analyzed using a software developed by ourselves based on programs to carry out all the operations indicated below, according to the procedure described by Frank (1989) with some modifications. Briefly, after a Gaussian smoothing of the optical density data, subtraction of the mean value, and centering of each individual image with respect to its center of mass, a typical image is selected to align all the other images in the set with respect to it, using iterative translational and rotational cross-correlation of every individual image with the typical image selected. Once all the individual images were aligned, each individual image was cross-correlated with all the rest of images in the set by a ±10 pixels translation and a ±10° rotation, obtaining image subsets for a given cross-correlation function maximum (from now on, called correlation coefficient *f* with values from 0 to 1) for each individual image. This provides us with translations, rotations, and correlation factors, which, together with those obtained before and during alignment, let us average the original images for each subset. Finally, the whole process is repeated with the original images, but now using as reference image the average image already obtained for each subset.

RESULTS

Characterization of the Monoclonal Antibodies Specific for the Fibrinogen Distal Domain. All murine antibodies isolated were of the IgG type, and their dissociation constants for fibrinogen binding were in the 0.1−1.0 nM range. All the selected antibodies (F2, F5, F6, F7, F8, F9, and F12) seemed to recognize the reduced and alkylated β chain of fibrinogen in blotting. All of the antibodies selected were directed to the distal nodules of the fibrinogen molecule, as observed by electron microscopy, but not all of them were equally useful for our purpose in the present work: to demonstrate unequivocally the arrangement of the C-terminal β domain of one-half of the fibrinogen molecule with respect to the same domain in the other half, based on the monoclonal character to the immunochemical probes used and on the dimeric nature of the fibrinogen molecule. Thus, F2, F5, and F8 produce mainly open or closed chains of fibrinogen monomers cross-linked through their distal domains at defined angles by the antibodies, which due to their large and variable size are unsuitable for image analysis. F6,

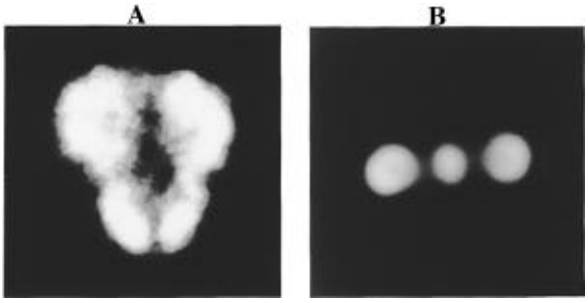

FIGURE 1: (A) Average image of the subset of IgG images with a correlation coefficient of 0.65, obtained by analysis of 200 individual electron microscopic images of IgG, as described in the Methods section. (B) Average image of the subset of fibrinogen images with a correlation coefficient of 0.90, after analysis of 174 individual electron microscopic images of fibrinogen.

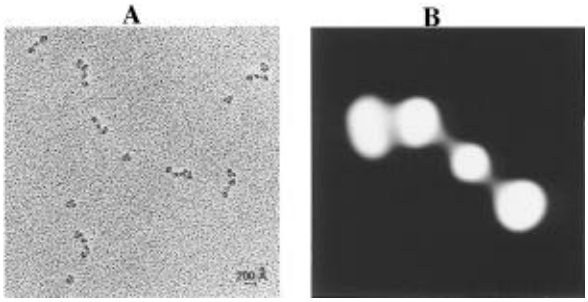

FIGURE 2: (A) Electron micrograph of the fibrinogen−F7 monoclonal antibody heterodimers after Pt/C rotary shadowing performed as described in the Methods section. Original magnification 150000× (reproduced at 45% of original size). Bar = 20 nm. (B) Average image of the subset of images of the heterodimers with a correlation coefficient of 0.80, obtained after analysis of 370 individual electron microscopic images of heterodimers.

F9, and F12 produce mainly complex aggregates, also unsuitable for image analysis. Finally, none of the antibodies inhibited fibrin formation.

Isolation of the Fibrinogen−Antibody Heterodimers and Heterotrimers. The SDS−PAGE analysis of the fractions of the Sephacryl S-400 column showed that the fibrinogen−antibody complexes eluted at the leading edge of the fibrinogen monomer fraction well separated from the free antibody fraction.

Images of the Monomers of Individual Monoclonal IgG and Fibrinogen. The analysis of 200 images of individual IgG molecules taken at random shows a large morphological variability among them, as expected due to their well-known flexibility (Yguerabide et al., 1970; Wade et al., 1989). Thus the prototypical image of the set (Figure 1A) correlates with 154 images for an $f = 0.60$; 80 images for $f = 0.65$; 27 images for an $f = 0.70$; and 4 images for an $f = 0.75$. On the other hand, and as expected (Montejo et al., 1992), the analysis of 174 images of individual fibrinogen molecules taken at random indicates a much more conserved and rigid morphology among them. Thus, the prototypical image of the set (Figure 1B) correlates with the following: all the rest of the images with an $f = 0.70$; 168 images with an $f = 0.80$; 128 images with an $f = 0.90$; 25 images with an $f = 0.95$; and 8 images with an $f = 0.97$.

Images of Fibrinogen−F7 Heterodimers. In the heterodimers the antibody is bound at one of the distal nodules of fibrinogen at an angle of about 45° with respect to the long axis of the molecule (Figure 2A). It could be expected that the binding of a monoclonal antibody to fibrinogen would restrict very severely the orientation of the molecule around its long axis, once it is laid down on the mica surface. However, this is not apparent from the analysis of 370 images of heterodimers. The prototypical image of the set (Figure 2B) correlates with the following: 370 images for an $f = 0.80$; 134 images for an $f = 0.90$; and 3 images for an $f = 0.95$.

In the average image of the subset corresponding to $f = 0.90$ (Figure 2B), it is apparent that the density at the antibody-free distal nodule appears asymmetrically distributed with respect to the long axis of fibrinogen, being slightly displaced toward the same site as the antibody.

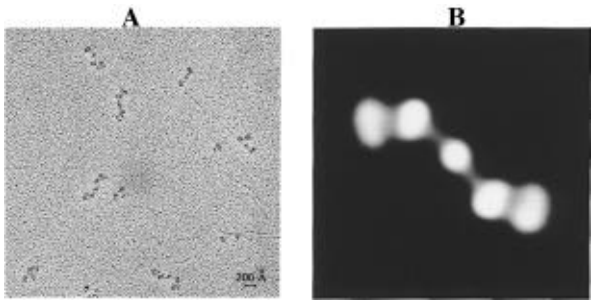

FIGURE 3: (A) Electron micrographs of the fibrinogen−F7 monoclonal antibody heterotrimers after Pt/C rotary shadowing. Original magnification 150000× (reproduced at 45% of original size). Bar = 20 nm. (B) Average image of the subset of images with a correlation coefficient of 0.85, obtained after analysis of 243 individual electron microscopic images of heterotrimers.

Images of Fibrinogen−$(F7)_2$ Heterotrimers. The heterotrimers show one antibody bound at each distal nodule of fibrinogen, oriented equally with respect to the long axis, as it is described above for the heterodimers, but at opposite sites with respect to it (Figure 3A).

By the same reasons as for the heterodimers, it could be expected that the two bound antibodies would restrict even more severely the orientation of fibrinogen around its long axis. Again, however, this is not apparent from the image analysis of 243 individual heterotrimers. The prototypical image of the set (Figure 3B) correlates with the following: 200 images for $f = 0.80$; 78 images for $f = 0.85$; and 11 images for $f = 0.90$. Here again, the density at the distal domains is slightly but asymmetrically distributed with respect to the long axis of fibrinogen, opposite to the antibody binding side at each domain.

DISCUSSION

Although not related with the main objective of the present work, it is remarkable how electron microscopy of metallically shadowed macromolecules, a very low resolution technique, when combined with image analysis is able to indicate the degree of overall molecular flexibility, as is the case here for IgG and fibrinogen, in good agreement with other techniques specially developed to assess molecular flexibility (Yguerabide et al., 1970; Montejo et al., 1992).

The relatively lower number of images in the subsets with high correlation coefficients for the fibrinogen−IgG heterodimers and heterotrimers, compared with the corresponding subsets for fibrinogen monomers, could be explained by the high flexibility introduced in the heterodimers and heterotrimers by the bound IgG molecules, making this contribution to the average images stronger than the severe restriction that bound IgG introduces in the orientation of fibrinogen around its long axis on the mica surface.

The main conclusion of the present work is that the epitopes for monoclonal antibody F7, located at the C-terminal end of the β chains of fibrinogen, are at the distal nodules equidistant from the center of the molecule and are arranged not colinearly with the long axis of the molecule but at opposite sides of it, i.e., following twofold symmetry. Thus, given the monoclonality of the antibodies used and the dimeric nature of the molecule, we can conclude that the distal domains of the two β chains are arranged in the same manner as these epitopes and, therefore, that the fibrinogen molecule has twofold symmetry. This symmetry pattern found here for the epitopes of F7 is the same as that found recently by Wiesel et al. (1992) for the platelet fibrinogen receptor binding sites located almost certainly at the C-terminal end of the γ chains. Attempts to obtain fibrinogen$-(F7)_n-(GPIIb/IIIa)_m$ heteropolymers to verify the expected symmetry pattern of the F7 epitopes with respect to the binding sites for GPIIb/IIIa have been unsuccessful so far.

Taken together, the twofold symmetry of fibrinogen in solution, unequivocally demonstrated here, and the overall rigidity of the molecule, demonstrated before (Montejo et al., 1992), point to the half-staggered double-strand model as the most probable model for fibrin polymerization, where each distal γ domain is linked to the complementary binding site in the central domain of a fibrin molecule in the neighbor strand of the same protofibril, exposed by the release of fibrinopeptide A, and to the distal γ domain of the neighboring molecule in the same strand. On the contrary, these features of fibrinogen do not support the interlocked single-strand model proposed before (Hunziker et al., 1990).

Originally, the binding sites of the activated platelet fibrinogen receptor on human fibrinogen were located at the C-terminal end of the γ chains (KQAGDV site), making these essential binding sites, and in the 95−98 and 572−574 stretches of the α chains (RGD sites) (Hawiger et al., 1989), with the α95−98 sequence constrained by flanking residues and not exposed in the soluble molecule. However, the interaction of fibrinogen with its platelet receptor through other sites in the molecule or the adsorption of fibrinogen on solid phase makes this sequence available for interaction (Ugarova et al., 1993). The twofold symmetry and the rigidity of fibrinogen provide two C-terminal ends of the γ chain in the trans position (Weisel et al., 1992) only available for cross-bridging receptors between neighbor platelets, except at plasma membrane folds within the same platelet. On the other hand, the availability of two additional RGD binding sites in the cis position with respect to each γ chain C-terminal site and at distances lower than 45 nm provides the possibility of secondary interactions with new receptors (Hawiger et al., 1989) moving laterally and rotationally (González-Rodríguez et al., 1994) in the vicinity, stabilizing further platelet−platelet aggregation and platelet adhesion to surfaces coated with fibrin or other adhesion proteins, cross-bridging neighbor receptors on the same platelet, and promoting receptor clustering (Polley et al., 1981) and a variety of other subsequent cellular phenomena.

ACKNOWLEDGMENT

We thank José M. Sánchez for his assistance in the metal shadowing of the samples, the maintenance of the electron microscope and with the photography, and M. Pérez for digitizing the images. We are thankful to Dr. J. C. Diaz-Masa for providing us with the Poros 20 polymeric column and advice on its use.

REFERENCES

Doolittle, R. F. (1984) *Annu. Rev. Biochem. 53*, 195−229.
Frank, J. (1989) *Electron Microsc. Rev. 2*, 53−74.
Friguet, B., Chaffote, A. F., Djavadi-Ohaniance, L., & Goldberg, M. E. (1985) *J. Immunol. Methods 11*, 305−319.
González-Rodríguez, J., Acuña, A. U., Alvarez, M. V., & Jovin, T. M. (1994) *Biochemistry 33*, 266−274.
Hall, C. E., & Slayter, H. S. (1959) *J. Biophys. Biochem. Cytol. 5*, 11−16.
Hawiger, J., Kloczewiak, M., Bednarek, M. A., & Timmons, S. (1989) *Biochemistry 28*, 2909−2914.
Hoeprich, P. D., & Doolittle, R. F. (1983) *Biochemistry 22*, 2049−2055.
Hunziker, E. B., Straub, P. W., & Haeberli, A. (1990) *J. Biol. Chem. 265*, 7455−7463.
Laemmli, U. K. (1970) *Nature (London) 227*, 680−685.
Markwell, M. A. K., Hass, S. M., Bieber, L. L., & Tolbert, N. E. (1978) *Anal. Biochem. 87*, 206−210.
Melero, J. A., & González-Rodríguez, J. (1984) *Eur. J. Biochem. 141*, 421−327.
Montejo, J. M., Naqvi, R. N., Lillo, M. P., González-Rodríguez, J., & Acuña, A. U. (1992) *Biochemistry 31*, 7580−7586.
Polley, M. J., Leung, L. L. K., Clark, F. Y., & Nachman, R. L. (1981) *J. Exp. Med. 154*, 1058−1068.
Rao, S. P. S., Poojary, M. D., Elliott, B. W., Melanson, L. A., Oriel, B., & Cohen, C. (1991) *J. Mol. Biol. 222*, 89−98.
Rivas, G. A., Aznárez, J. A., Usobiaga, P., Saiz, J. L., & González-Rodíguez, J. (1991) *Eur. Biophys. J. 19*, 335−345.
Towbin, H., Staehelin, T., & Gordon, J. (1979) *Proc. Natl. Acad. Sci. U.S.A. 76*, 4350−4354.
Ugarova, T. P., Budzynski, A. Z., Shattil, S. J., Ruggeri, Z. M., Ginsberg, M. H., & Plow, E. F. (1993) *J. Biol. Chem. 268*, 21080−21087.
Veklich, Y. I., Gorkun, O. V., Medved, L. V., Nieuwenhuizen, W., & Weisel, J. W. (1993) *J. Biol. Chem. 268*, 13577−13585.
Wade, R. H., Taveau, J. C., & Lamy, J. N. (1989) *J. Mol. Biol. 206*, 349−356.
Weisel, J. W., Stauffacher, C. V., Bullit, E., & Cohen, C. (1985) *Science 230*, 1388−1391.
Weisel, J. W., Nagaswami, C., Vilaire, G., & Bennet, J. S. (1992) *J. Biol. Chem. 23*, 16637−16643.
Yguerabide, J., Epstein, H. F., & Stryer, L. (1970) *J. Mol. Biol. 51*, 573−590.

BI950858E